GA–A27393

# IMPURITY MIXING IN MASSIVE-GAS-INJECTION SIMULATIONS OF DIII-D

by
V.A. IZZO

OCTOBER 2012

GENERAL ATOMICS

# DISCLAIMER

GA–A27393

# IMPURITY MIXING IN MASSIVE-GAS-INJECTION SIMULATIONS OF DIII-D

by
V.A. IZZO*

This is a preprint of a paper to be presented at the Twenty-fourth IAEA Fusion Energy Conf., October 8-13, 2012 in San Diego, California.

*University of California San Diego, San Diego, California.

Work supported by
the U.S. Department of Energy
under DE-FG02-95ER54309

GENERAL ATOMICS PROJECT 03726
OCTOBER 2012

# Impurity Mixing in Massive-Gas-Injection Simulations of DIII-D

V.A. Izzo

University of California-San Diego, La Jolla, California, 92093, USA

*E-mail contact of main author: izzo@fusion.gat.com*

**Abstract.** Both mixing efficiency and toroidal radiation peaking are studied in a series of NIMROD MHD simulations of massive gas injection in DIII-D. In the simulations, the toroidal localization and poloidal injection location of the Ne source are varied. The primary finding is that both mixing and toroidal peaking are strongly dependent on the phase of the m=1/n=1 mode that is destabilized by the gas injection — in particular on the relationship between that phase and the injection location. In fact, the location of the toroidal peak in the radiated power is independent of the toroidal source location (they may diametrically opposed), and is determined only by the 1/1 mode phase. Results for runaway electron confinement during these simulations are also reported, with some enhancement in runaway electron deconfinement seen for high-field-side injection.

## 1. Introduction

The design for the ITER disruption mitigation system (DMS) will be finalized in 2016, with the number and location of ports dedicated to the DMS being chosen in 2013. The port selection will be constrained largely by the need to maintain radiation asymmetry below an acceptable threshold, which will almost certainly be exceeded if material is injected from only a single toroidal location. A fast, highly localized radiative shutdown of ITER could easily result in significant melting of the ITER first wall [1], so the DMS must be a high priority system. Still, every port allocated to the DMS comes at the expense of other systems, so a strong scientific basis must be established for the number of ports needed to prevent machine damage. While a large quantity of massive gas injection (MGI) data has been collected on a variety of tokamaks, studies varying MGI injector location and symmetry are less abundant. A few exceptions include MGI experiments done with multiple toroidal ports on Alcator C-Mod [2] and comparison of low-field- and high-field-side MGI on ASDEX Upgrade [3]. Because gas jets in particular do not deeply penetrate into the plasma (e.g., relative to pellets), assimilation of the gas jet material into the plasma core (often referred to as "mixing efficiency") depends substantially on large scale flows generated in part by macroscopic MHD instabilities. Beyond overall assimilation, these non-symmetric flows will partially determine (in conjunction with injector locations) the impurity distribution and asymmetry (and thus radiation asymmetry) during the thermal quench (TQ) phase. Here we present MHD simulations of impurity mixing during MGI in DIII-D in order to better understand how gas injection location interacts with MHD instabilities to determine the impurity distribution in the TQ and current quench (CQ).

## 2. NIMROD Model

The NIMROD [4] code is a 3D extended-MHD code which has an option for an impurity species, including ionization, recombination and radiation cooling [5]. The impurity species

in all of the present simulations is Ne, which is a major candidate for MGI in ITER. The code evolves equations for all three components of magnetic field and fluid velocity, along with a single temperature, and 12 continuity equations for deuterium ions plus every charge state of Ne including neutrals. The electron density is determined by quasi-neutrality. The simulations are initiated with an EFIT equilibrium reconstruction of a DIII-D discharge (#137623), and a prescribed spatial distribution of neutral Ne is introduced. The simulation domain extends beyond the separatrix (the computational boundary is a smoothed version of the DIII-D wall), and, in each of the simulations presented here, the initial Ne profile is strongly concentrated at the edge of the domain, with most of the Ne deposited outside the separatrix. The Ne gradually diffuses/mixes into the plasma region and cools the plasma edge, eventually triggering a TQ.

For numerical efficiency the resistivity of the hot core plasma must be artificially enhanced. To this end, the expression for the resistivity — only in the Ohm's law — is modified to contain a "cutoff" Temperature: $\eta\ (T) = \eta_{Spitzer}\ [\min(T, 100\ eV)]$. This modified expression is not used when calculating the resistivity in the Ohmic heating term of the energy equation (the normal Spitzer expression is used), therefore the correct balance between radiation and Ohmic heating is maintained. This approximation will have two primary consequences: 1) a loss of energy from the system will occur because the magnetic energy dissipated Ohmically is greater than the thermal energy produced; 2) reconnection will be faster in the hot core than the resistive MHD model would predict. The first consequence is acceptable because a very large fraction of the Ohmic dissipation will occur in the regions of the plasma that have already reached TQ-like temperatures (<10 eV), whereas the power imbalance occurs only in regions of the plasma with $T > 100$ eV, where the Ohmic dissipation is small on the TQ time scale. (By the end of the TQ, $T < 100$ eV everywhere, and $\eta = \eta_{Spitzer}$ everywhere). The second consequence has some physical justification, since the core plasma will be in the collisionless regime, in which we expect faster reconnection than resistive MHD would predict (absent a very well resolved reconnection layer) and a reconnection rate independent of resistivity [6].

Four simulations (A-D) are carried out in which the spatial distribution of injected neutral Ne is varied (Fig. 1). In simulation A, the Ne source is poloidally and toroidally symmetric, so that a mantle of Ne gas initially surrounds the entire plasma. In simulations B and C, the Ne in injected primarily on the low-field-side (LFS) of the domain, and is toroidally peaked in each case, with simulation C more strongly toroidally peaked than B. Finally, simulation D has the Ne injected primarily on the high-field-side (HFS), with the same toroidal peaking as simulation B.

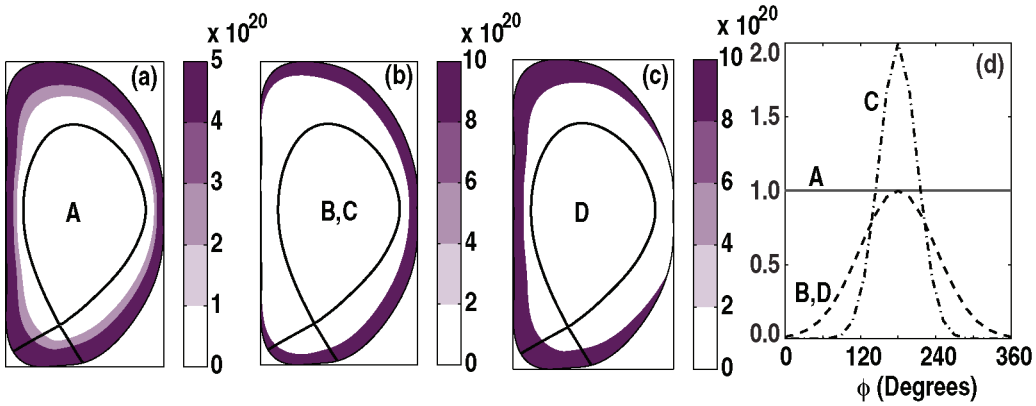


*FIG. 1. (a-c) Poloidal contours of injected Ne density for simulations A-D. (d) Toroidal variation of injected Ne for the four simulations.*

## 3. Simulation Results

### 3.1. Thermal quench onset

The four simulations can be divided into three phases, the pre-TQ, TQ and CQ phases, where each simulation is carried out well past the end of the TQ phase, but not to the end of the CQ. The onset of the TQ is characterized by a significant increase in the loss rate of the thermal energy [Fig. 2(a)] which occurs as the MHD modes become large and destroy flux surfaces. Although a majority of the thermal energy is lost during the pre-TQ in these simulations, the central $T_e$ does not drop significantly until the TQ onset. The TQ onset time is larger in simulation A (~1.5 ms) than in every other simulation (<1.0 ms). This is likely due to the pre-existence of a large $n$>0 perturbation in simulations B-D leading to earlier instability onset and faster mode saturation.

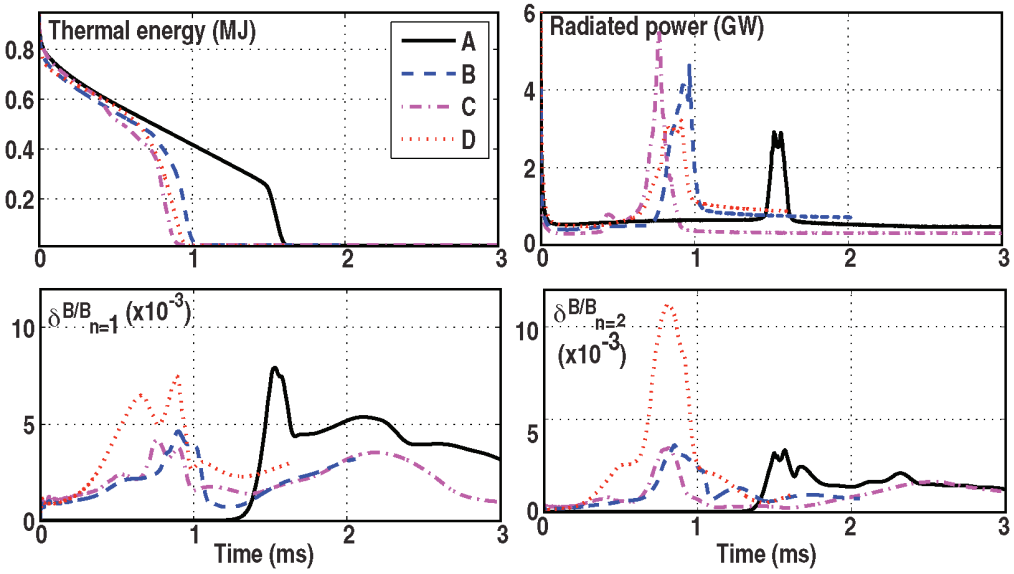


*FIG. 2. Time histories for four simulations of (a) stored thermal energy, (b) radiated power, and (c) n=1 and (d) n=2 fluctuating field amplitudes.*

Injection on the LFS (B and C) produces the strongest radiated power flash of about 5 GW. The smaller flash in the symmetric injection case can be attributed to the lower stored thermal energy at the time of TQ onset, the HFS injection case has a slightly broader radiation peak than the other cases. The two LFS injection simulations also have very similar MHD behavior, as seen in the $n$=1 and $n$=2 mode amplitude plots in Fig. 2(c) and 2(d). Simulation D is only simulation to exhibit a dominant $n$=2 mode, which reaches very large amplitude and contains both 3/2 and 2/2 components.

### 3.2. Mixing efficiency

Mixing efficiency can be defined various ways experimentally, but is generally a number measuring the assimilation of injected gas into the plasma. In DIII-D, it has been defined as the total ionized impurities within the plasma volume divided by the total gas injected through the valve; this value can range from a few percent to a few tens of percent [7]. Unlike MGI experiments, where diagnostics cannot account for all of the injected gas at all times, all of the Ne deposited in the simulation domain remains there either as ions or neutrals. Still, in our simulations less than three percent of the deposited Ne is initially inside the separatrix, and this fraction increases with time due to both advection and diffusion, so we can define a comparable mixing efficiency as the ratio of Ne inside the separatrix to Ne in the entire domain; we call this $Y_{\mathrm{mix,sep}}$. We are also specifically interested in the mixing of impurities into the core, so we calculate a second quantity, $Y_{\mathrm{mix,50}}$, which measures the fraction of total Ne which is inside the 50% flux surface ($\psi_n$=0.5). Both of these quantities are plotted as a function of time in Fig. 3.

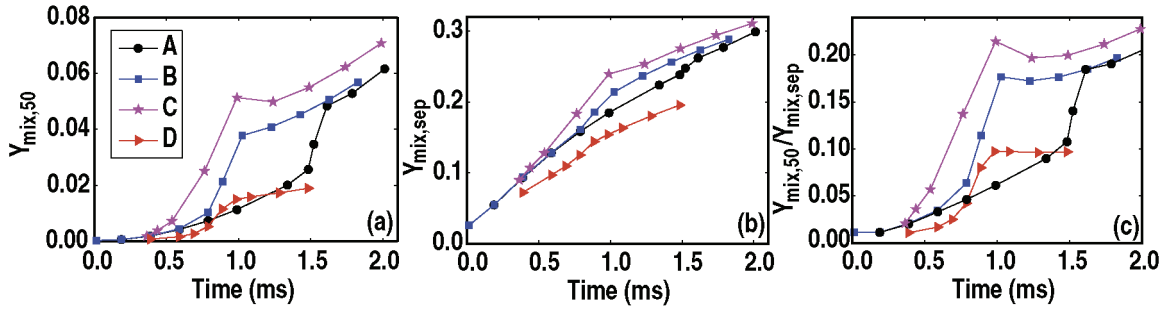


*FIG. 3. (a) Fraction of total injected Ne that is inside the 50% flux surface ($Y_{mix,50}$). (b) Fraction of total injection Ne that is inside the separatrix ($Y_{mix,sep}$). (c) Ratio of $Y_{mix,50}$ to $Y_{mix,sep}$..*

The transport of impurities across the separatrix is dominated by diffusion, due to the sharp Ne gradient imposed by the Ne source profile. Consequently, $Y_{\mathrm{mix,sep}}$ behaves quite similarly as a function of time in every case, with a slightly reduced assimilation in HFS injection simulation (D). The latter effect may be due to geometry effects and the particular choice of poloidal source profile — for instance, very concentrated sources at the outboard and inboard midplane might behave more similarly. However, a clear variation is seen in the behavior of $Y_{\mathrm{mix,50}}$ which is not dominated by diffusion, but rather has a large contribution

from advection associated with the MHD modes. In each case, we can see that $Y_{mix,50}$ rises slowly until the onset of the TQ, then increases sharply at that time. Again, the effect is less dramatic for simulation D. To partially separate out the two effects — reduced diffusion across the separatrix and reduced MHD mixing — we plot the ratio $Y_{mix,50}/ Y_{mix,sep}$ in Fig. 3(c). MHD mixing appears to be roughly half as effective in simulation D. As will be shown in the next section, this result does not necessarily point to the conclusion that HFS injection produces less efficient mixing.

### 3.3. Radiation asymmetry

Examination of the toroidal asymmetry of the radiated power yields several surprising findings. In Fig. 4(a), the torus is divided into 32 toroidal sections and the total radiated power in each segment is calculated. For each simulation this is done at the time when the total radiated power is a maximum during the TQ. The toroidal peaking factor (TPF) is calculated as the peak value over the average value [Fig. 4(a)]. First, we note that none of the TPF values are very severe — all are below two. But, even with an idealized, perfectly symmetric gas source (simulation A), some toroidal peaking occurs. The asymmetry occurs because flows associated with the m=1/n=1 mode play a predominant role in convecting heat from core to edge and particles from edge to core.

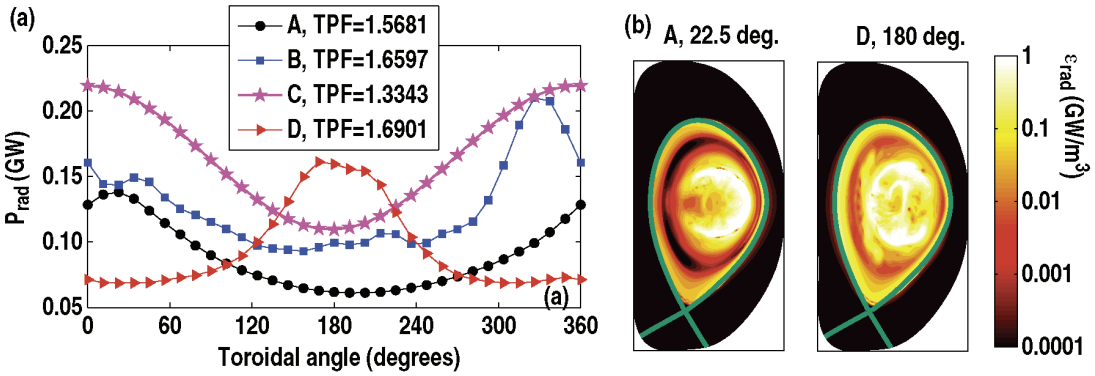


*FIG. 4. (a) Radiated power as a function of toroidal angle for the four simulations. Contours of emissivity for simulations A (b) and D (c) are shown at the toroidal peak in each case.*

The most toroidally peaked source (simulation C), has the lowest TPF. Even more unexpected, the toroidal maximum in the radiated power occurs at 0°, whereas the Ne source was peaked at 180°. Further, the maximum toroidal peaking factor occurs for the HFS injection simulation (D). Also, only this simulation has the radiated power peaked at 180°, where all the others are peaked near 0°.

Each of these observations can be explained in a coherent picture when it is noted that the 1/1 mode is found to have nearly the same phase in every simulation (the mode and plasma do not rotate). In every case, the 1/1 flow pattern is such that the flow at the midplane is in the outward major radial direction at 0° and the inward major radial direction at 180°, as illustrated in the cartoon in Fig. 5. Now, the mode convects heat from the core to the edge and particles from the edge to the core. But, as illustrated in Fig. 5(a), the LFS particle source is toroidally peaked where the 1/1 flow is inward toward the core, which maximizes particle mixing. The HFS source [Fig. 5(b)] is peaked where the flow is outward. The radiated power peak is produced primarily by the flow of heat from the core to the impurity-dense edge. For instance, in Fig. 4(b), we see that the radiated power is poloidally peaked on the outboard side near 0° for the symmetric source simulation. So, with the LFS source, the maximum outward heat flow aligns with the minimum Ne density, producing less toroidal peaking than the HFS source, for which the maximum heat flow aligns with the maximum Ne density.

Of course, the picture in Fig. 5 is simplified, and neglects in particular the presence of other modes and of heat transport along stochastic field lines produced by those modes, which also contributes the radiated power flash during the TQ. Still it explains the major observations from both Figs. 3 and 4, including those that appear counter-intuitive. Most importantly, the poor mixing in simulation D appears to be unrelated to the fact of HFS injection. A similar simulation with the source at 0° would provide a more fair comparison with the LFS injection cases.

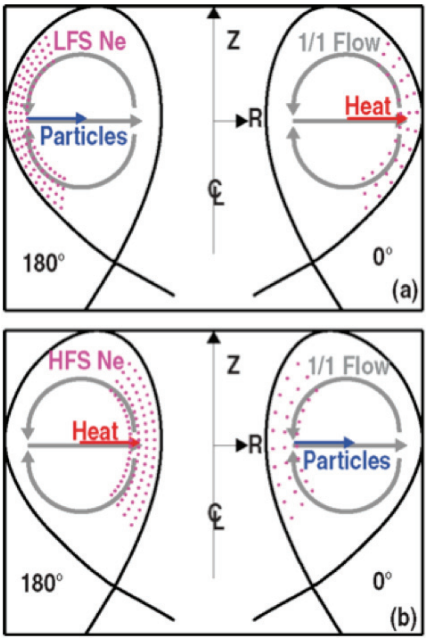


*FIG. 5. Cartoon of heat and particle flux due to the 1/1 mode, which aligns differently with the toroidal Ne peak for LFS injection (a) and HFS injection (b).*

### 3.4. Runaway electron losses

In each simulation a trace population of runaway electron (RE) orbits is tracked to compute the confinement of REs when the fields become stochastic. These are merely test particles, initiated at $t$=0 with random poloidal and toroidal locations in the confined volume and specified energies that are suprathermal but not highly relativistic. More details on the RE model can be found in [8]. In each of these simulations 2109 RE orbits are tracked. Results for all four simulations appear in Fig. 6(a), showing the fraction of the initial seed that remains confined as a function of time. In the hot core there is initially no runaway threshold, and seeded electrons in that region will gradually lose energy and may eventually thermalize. For the symmetric injection simulation (A) about 30% of the seed thermalizes, so we plot

both the total confined population, and the confined suprathermal population as dashed and solid lines, respectively. Thermal electrons generally orbit too slowly to be lost during the TQ.

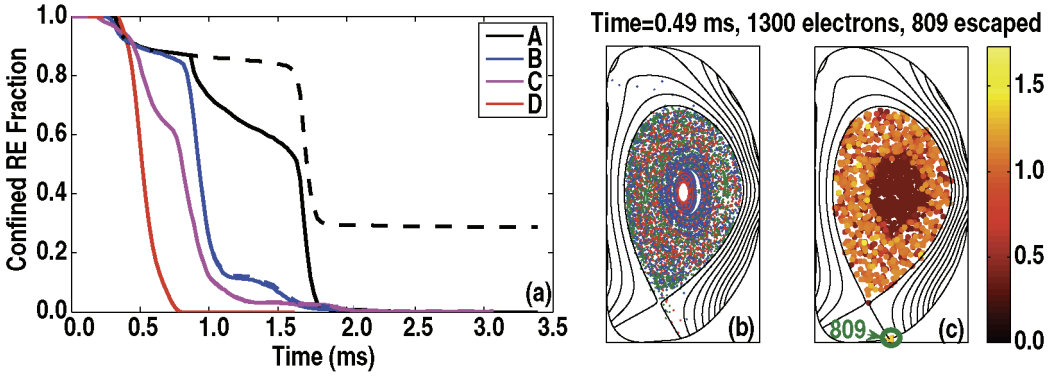


*FIG. 6. (a) Confined fraction of runaway seed vs time; dashed line is all seed electrons, solid line is only suprathermal electrons. (b) Magnetic field puncture plot for simulation D at 0.49 ms. (c) Poloidal locations of 1300 confined REs at 0.49 ms, and striking location of lost REs. Colors are RE energy in MeV.*

In each of these simulations, nearly the entire seed population of REs is lost. In three cases, the timing of the rapid RE loss event is co-incident with the TQ onset. We can easily understand that the same flux surface destruction that dumps heat from the plasma also dumps fast electrons. However, in simulation D, the RE losses immediately precede the TQ, which occurs at the same time as in simulations B and C. The very prompt "prompt-loss" of REs in simulation D can be understood in light of the early large peak that appears in the $n$=1 mode. This mode destroys the outer flux surfaces and appears to highly distort the core flux surfaces to a sufficient degree to deconfine all of the REs by 0.8 ms, while the core flux surfaces remain sufficiently intact to delay a core TQ slightly. With overall similar RE confinement results in every case, we can not conclusively determine whether HFS injection has better RE deconfinement properties without a larger set of simulations.

## 4. Conclusions

The primary aim of these simulations was to study how particle mixing and radiated power asymmetry during MGI are affected by the location and localization of gas injection. The results show that the phase of m=1/n=1 mode plays a predominant role in determining both mixing efficiency and toroidal peaking factor. In fact, the location of the toroidal radiation peak appears entirely independent of the Ne gas source location, and only dependent on the 1/1 mode phase, sometimes producing a peak 180 degrees away from the source. Both the mixing efficiency and TPF are determined by the phase relationship between the Ne source and the 1/1 mode. As it happens, the phase relationship that minimizes TPF also maximizes mixing efficiency, both of which are desirable outcomes.

From these results we cannot draw conclusions about the relative merits of HFS or LFS injection, since in one case the mode was phase aligned with the source and in the other it was anti-aligned. We expect that if the sources are moved to the opposite toroidal location, mixing efficiency would improve in the HFS injection simulation, and be significantly degraded for LFS injection. When these additional simulations are completed, we can make a fair comparison of poloidal injection locations, but those are left to future work. The poloidal injection location does appear to qualitatively impact the MHD evolution, for instance producing a very large $n$=2 mode in the HFS injection simulations that does not appear in the others. HFS injection may also be preferable for RE deconfinement, although a larger set of simulations is again required to draw definite conclusions.

In the NIMROD simulations the plasma and the mode do not rotate. MGI generally slows plasma rotation significantly in experiments, but any residual rotation that was fast relative to the TQ time scale might render these results less relevant experimentally. On the other hand they may be relevant if the mode is locked. It is a peculiarity of the simulations that the mode always takes on the same phase (probably due to the non-random initial perturbation), although it is not inconceivable that a mode could consistently lock at the same phase in a real tokamak due to error fields or device asymmetries. Whether the $n$=1 mode phase could be playing a role, either systematically or randomly, in single location gas jet experiments is a proposition which will need to be considered in greater detail.

This work was supported by the US Department of Energy under DE-FG02-95ER54309.

## References

[1] ITER Physics Expert Group on Disruptions, Plasma Control, and MHD, *et al.,* Nucl. Fusion **39** (1999) 2251.
[2] GRANETZ, R.S., *et al.,* Bull. Am. Phys. Soc. **56** (2011) 334.
[3] PAUTASSO, G., *et al.*, "Massive gas injection from the high field side of ASDEX Upgrade," Proc. 38th EPS Conference on Plasma Physics, Strasbourg, 2011, http://ocs.ciemat.es/EPS2011PAP/html/author.html, paper P4.108.
[4] SOVINEC, C.R., *et al.,* J. Comput. Phys. **195** (2004) 355.
[5] IZZO, V.A., *et al.,* Nucl. Fusion **51** (2011) 063032.
[6] HUANG, Yi-Min and BHATTACHARJEE, A., Phys. Plasmas **17** (2010) 062104.
[7] HOLLMANN, E.M., *et al.,* Nucl. Fusion **48** (2008) 115007.
[8] IZZO, V.A., *et al.,* Nucl. Fusion **51** (2011) 063032.